JOURNAL OF SPACECRAFT AND ROCKETS
Vol. 44, No. 1, January–February 2007

Enhancement in Optimal Multiple-Burn Trajectory Computation by Switching Function Analysis

Yunjun Xu*
University of Oklahoma, Norman, Oklahoma 73019

DOI: 10.2514/1.25082

This paper describes an improvement in designing a real time optimal multiple-burn trajectory that should be rapid and adaptive. The computational cost for solving a multiple-burn trajectory problem comes from 1) trajectory propagation (or simulation of a trajectory) and 2) trajectory iterations (or computation of gradient information). Tremendous work has been done to reduce this cost, especially in the area of increasing the solution convergence or gradient calculation speed. However, in applications such as an orbit-to-orbit transfer, a long range payload delivery, or a medium or low thrust-to-weight ratio trajectory, the propagation time of the coast arc is the dominant one of the computational cost, and thus several studies have been focused on solving this problem by using parallel computing techniques. In this paper, through an oscillation frequency study of the switching function, the propagation of the coast arc is avoided and "safely" replaced by a zero-finding program. Using this method, the speed of the real time trajectory design is increased. Numerical implementation issues of this algorithm are discussed in detail. To show the effectiveness of the proposed algorithm, four trajectory designs have been simulated: two Hohmann-type orbital transfers, a low Earth orbital insertion, and the McCue problem. Atmospheric drag and J_2 perturbations have been considered in these simulations.

Nomenclature

A	=	vehicle's cross-section area, m^2
a	=	orbital semimajor axis, m
$\mathbf{a}_{\text{drag}}$	=	atmospheric drag acceleration, m/s^2
$\mathbf{a}_i$, $i = 1, \ldots, 13$	=	constant vectors in the switching function
$\mathbf{a}_{J_2}$	=	J_2 acceleration, m/s^2
C_D	=	drag coefficient
c	=	nozzle exit velocity, m/s
c_i, $i = 1, 2$	=	constants defined for $\mathbf{a}_{\text{drag}}$ and $\mathbf{a}_{J_2}$
e	=	orbital eccentricity
F_i, $i = 1, \ldots, 6$	=	modes of the switching function
$\mathbf{H}$, H	=	orbital angular momentum and its corresponding magnitude, m^2/s
H_a	=	Hamiltonian function
h	=	altitude, m
$\mathbf{I}$	=	identity matrix
J	=	performance index
J_2	=	J_2 constant
m	=	mass of a vehicle, kg
p	=	orbital semilatus rectum, m
R_e	=	Earth radius, m
$\mathbf{r}$, r	=	position vector and its magnitude in the Earth frame, m
S	=	switching function
T	=	booster thrust, N
t	=	time, s
$\mathbf{v}$, v, $\hat{\mathbf{v}}$	=	velocity, its magnitude, and unit vector in the Earth frame, m/s
x, y, z	=	sidereal or nonrotating x axis, y axis, and z axis, m
$\hat{z}$	=	z unit direction in the Earth frame
θ	=	orbital true anomaly, rad
$\boldsymbol{\lambda}_R$, $\boldsymbol{\lambda}_V$, λ_m	=	costates
μ	=	Earth gravitational parameter
ρ	=	atmospheric density, kg/m^3
ω	=	orbital argument of periapsis, rad
$\mathbf{1}_b$	=	booster thrust direction

Subscripts

des	=	desired
f	=	final
i, j	=	elements of a matrix
max	=	maximum
sampled	=	sampled point
Tol	=	tolerance
zero	=	zero point for the switching function
0	=	initial condition
1, 2, 3	=	components of a vector

Superscripts

T	=	matrix transpose
*	=	optimum

Introduction

TRAJECTORY optimization problems have been investigated extensively and increasingly more papers have been published since the 1950s. Lawden's design [1,2] of optimal spacecraft trajectories led to the primer-vector theory, and many other results [3–8] afterward have been variations of the fundamental Pontryagin maximum principle [9]. Bell [10], Lawden [11], and more recently Betts [12] and Ocampo [13] have collected most of the important contributions in optimal trajectory design and related numerical techniques which have been used to solve the unavoidable two-point-boundary-value problem (TBVP). It is well known that the optimal solution of TBVPs is extremely sensitive to the initial primer (costate) vector, and to find even a partial closed-form solution for such a problem [14] is difficult. Numerical methods for computing the optimal orbit trajectory are typically categorized into direct [15–17], indirect [14], or hybrid methods [18,19]. The aforementioned optimal trajectory design methodologies have been widely used in aircraft [15], launch vehicles, and space vehicles [20], with single or multiple-burn arcs. In some mission scenarios, a multiple-burn trajectory is superior to a single-burn trajectory in terms of fuel

Presented at the AIAA Guidance, Navigation, and Control Conference, Keystone, Colorado, 21–24 August 2006; received 10 May 2006; revision received 5 September 2006; accepted for publication 5 September 2006.

*Assistant Professor, School of Aerospace and Mechanical Engineering; yjxu@ou.edu. AIAA Member.

consumption. Furthermore, a multiple-burn trajectory guidance law increases the vehicle's autonomy and performance. For example, launch locations will not be detected as easily as they would be in a single-burn ballistic-type trajectory.

A multiple-burn trajectory may include multiple burn and coast segments. The basic segment is a trajectory arc that connects two nodes [13]. This arc can be an uncontrolled ballistic arc (coast arc) or a controlled arc (burn arc). In designing such a multiple-burn optimal trajectory, the computational cost comes from 1) a relatively high cost in trajectory propagation (simulation of a trajectory) and 2) the number of trajectories (computation of gradient information) that have to be iterated in finding the optimal solution [21,22].

Much research has been done to reduce the computational cost in finding the optimal solution for multiple-burn trajectories. Related publicly available literatures can be categorized into two groups: those that increase the speed associated with gradient calculations and those that increase the speed in coast arc propagation. Most of them [7,23–29] have been focused on finding analytical or hybrid gradient information for multiple-burn trajectories [23–27] or analyzing the second variation theory [29].

However, the computational cost in coast arcs propagation has been shown to be dominant in many scenarios [30]. Brusch [22] mentioned in his paper that trajectory optimization problems that integrate the equations of motion usually fail to meet the low cost requirement. Up until now, much research has been done to reduce the computational cost in coast arcs. First, with the assumption of a Keplerian model, analytical solutions [31–36] of the coast arc are found in different forms to avoid integrations and help in deriving analytical Jacobian matrices for iterations. Second, by investigating the transversality and necessary conditions associated with the switching function in a coast arc, the numerical propagation of certain states and costates, such as mass and mass related costate [30], is eliminated. Third, parallel computing techniques [21,37] have been introduced into multiple-burn trajectory designs.

The techniques mentioned above greatly increase multiple-burn trajectory optimization progress. However, the key aspect related to the computational cost, propagating the coast arc, remains. To avoid the coast arc propagation, the end times of coast arcs are typically considered as parameters for optimization [14,30]. In Brown's report [23], he demonstrated that the trajectory finding time is 50% less when compared to the cases in which states are directly propagated. Nevertheless, when using this method the size of the Jacobian matrix will be increased. Thus, as discussed later, the iteration will be longer and the optimal solution will be more sensitive to the initial costate guess.

In the multiple-burn trajectory design, the function which governs the switching time (or location) from a burn arc to a coast arc or from a coast arc to a burn arc is the so-called "switching function." Typically, the switching time can be solved from zero-finding programs. However this property is rarely used to avoid the propagation of coast arcs. The reason is, we need to find the *first* zero without a good initial guess. In 1989, Carter [38] mentioned in his paper that the switching function either has a finite number of zeros (when the eccentricity is larger than zero) on a closed bounded interval or it is identically zero (when the eccentricity equals zero). To use zero-finding algorithms, this theorem is still not safe because of the zero leakage that may happen when finding the switching locations as illustrated in Fig. 1. The axis in Fig. 1 can be the time or orbital true anomaly.

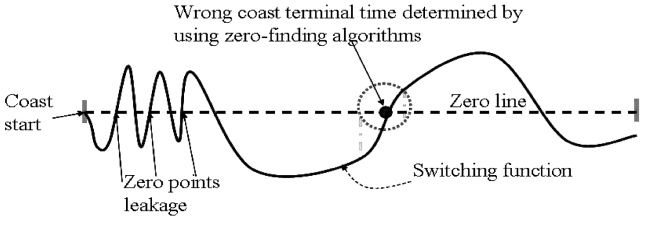

Fig. 1 A schematic demonstration of the zero leakages.

The purpose of this paper is to find the maximum oscillation frequency associated with the switching function for a vehicle experiencing Keplerian motion. Also, numerical issues in applying this technique will be discussed and the reduction in the computational cost will be analyzed coarsely and demonstrated using numerical examples. The advantages are obvious: 1) the coast arc propagation is avoided and the computational time for the coast arc is dramatically reduced; 2) using the coast arc's terminal time as an optimization parameter is avoided; and 3) a better precision can be achieved using zero-finding algorithms instead of using propagation methods. If the coast arc is directly propagated, the precision of the found switching time is determined by the propagation step size.

This paper is organized as follows. First, the dynamic models of the basic segments are listed. Second, the switching function in the multiple-burn trajectory is studied and a lemma is proven to show that the maximum oscillation frequency of a switching function in a noncircular orbit is eight with respect to a sinusoid-type wave. After that, a summary of the algorithm for quickly finding the terminal time of a coast arc is discussed. Next, the effectiveness of the proposed algorithm is shown through the simulation of four trajectory designs: two Hohmann-type orbital transfers (one high and one medium thrust-to-weight ratio), a low Earth orbital insertion, and the McCue problem [39]. Atmospheric drag and J_2 perturbations have been considered in these numerical simulations. Finally, a conclusion is given.

Basic Segment Dynamics and Optimal Trajectory Control

In multiple-burn trajectories, a basic segment is a trajectory arc that connects two points. The initial and final times (fixed or free) at these two nodes are referred to as t_0 and t_f, respectively. The thrust T is bounded as $T \in [0, T_{\max}]$ and the direction of the thrust vector $\mathbf{1}_b$ is optimally controlled.

Burn Arc Formulation

The state vectors $\mathbf{r}$, $\mathbf{v}$, and m (position, velocity, and mass) along a burn arc are governed by Eq. (1). $\mathbf{a}_{\text{drag}}$ and $\mathbf{a}_{J_2}$ are included.

$$\begin{bmatrix} \dot{\mathbf{r}} \\ \dot{\mathbf{v}} \\ \dot{m} \end{bmatrix} = \begin{bmatrix} \mathbf{v} \\ -(\mu/r^3)\mathbf{r} + (T/m)\mathbf{1}_b + \mathbf{a}_{J_2} + \mathbf{a}_{\text{drag}} \\ -T/c \end{bmatrix} \tag{1}$$

The J_2 effect [40] [Eq. (2)] comes from the sectoral variation of the Earth density, where $c_1 \triangleq -\mu J_2 R_e^2$, $J_2 = 0.00108263$, r, z, and $\hat{z}$ are the vehicle's position magnitude, the z component, and the unit vector in the Earth coordinate system, respectively. The J_2 perturbation causes the orbital shape to be changed slowly:

$$\mathbf{a}_{J_2} = c_1\{[3/(2r^5) - 15z^2/(2r^7)]\mathbf{r} + 3z/(r^5)\hat{z}\} \tag{2}$$

A NASA density model (NASA Glenn Simple Model[†]) is used as shown in Eq. (3), where $h = r - R_e$, $\xi = -131.21 + 0.00299h$, and $\zeta = 2.488[(\xi + 273.1)/216.6]^{5.256}$. The atmospheric drag model is shown in Eq. (4), where A is a vehicle's cross-section area, $\hat{\mathbf{v}}$ is the unit vector of the velocity, and $c_2(\mathbf{r}) \triangleq -[1/(2m)]\rho C_D A$.

$$\rho(h) = \zeta/[0.2869(\xi + 273.1)] \qquad h \geq 25 \text{ km} \tag{3}$$

$$\mathbf{a}_{\text{drag}} = c_2(\mathbf{r})\|\mathbf{v}\|\mathbf{v} \tag{4}$$

A simplified drag coefficient model is modified based on Anderson [41]:

$$C_D = 2 \quad \text{if } \|\mathbf{v}\| \geq 340 \text{ m/s} \tag{5}$$

[†]"Earth Atmosphere Model—NASA GRC," data available on-line at http://www.grc.nasa.gov/WWW/K-12/airplane/atmosmet.html [retrieved 2 May, 2006].

Coast Arc Formulation

Without thrusts, Eq. (6) is the equation of motion for a spacecraft in a coast arc. Coast arcs usually happen outside of the atmospheric region, but for general use, we still include the J_2 perturbation and the atmospheric drag in the model:

$$\begin{bmatrix} \dot{\mathbf{r}} \\ \dot{\mathbf{v}} \end{bmatrix} = \begin{bmatrix} \mathbf{v} \\ -(\mu/r^3)\mathbf{r} + \mathbf{a}_{J_2} + \mathbf{a}_{\text{drag}} \end{bmatrix} \tag{6}$$

Neglecting the atmospheric drag and the J_2 perturbation, the analytical solution of the coast arc has been solved by Glandorf [31].

Hamiltonian and Switching Functions

The Hamiltonian function is shown in Eq. (7) with costates $\boldsymbol{\lambda}_R, \boldsymbol{\lambda}_V$, and λ_m. The optimal condition is listed in Eq. (8) and can be simplified to the well-known result $\mathbf{1}_b^* = \boldsymbol{\lambda}_V^*/\|\boldsymbol{\lambda}_V^*\|$. The switching function is defined as $S \triangleq \boldsymbol{\lambda}_V^T \mathbf{1}_b/m - \lambda_m/c$. For simplicity, we can neglect the superscript * in the optimal thrust direction $\mathbf{1}_b^*$. The burn and coast arc switching points are derived as Eq. (9). When the switching function value equals zero at all time (the orbital eccentricity is zero [38]), it is a singular arc:

$$H_a = \boldsymbol{\lambda}_R^T \mathbf{v} + \boldsymbol{\lambda}_V^T[-(\mu/r^3)\mathbf{r} + \mathbf{a}_{J_2} + \mathbf{a}_{\text{drag}}] + T\left(\boldsymbol{\lambda}_V^T \mathbf{1}_b/m - \lambda_m/c\right) \tag{7}$$

$$H_a^*\left(\boldsymbol{\lambda}_R^*, \boldsymbol{\lambda}_V^*, \lambda_m^*, \mathbf{r}^*, \mathbf{v}^*, m^*, \mathbf{1}_b^*\right) \geq H_a\left(\boldsymbol{\lambda}_R^*, \boldsymbol{\lambda}_V^*, \lambda_m^*, \mathbf{r}^*, \mathbf{v}^*, m^*, \mathbf{1}_b\right) \tag{8}$$

$$T = \begin{cases} 0 & S \leq 0 \\ T_{\max} & S > 0 \end{cases} \tag{9}$$

The costate dynamics ($T = 0$ for coast arcs) is written as

$$\dot{\boldsymbol{\lambda}}_V = -\boldsymbol{\lambda}_R - \mathbf{A}_1 \boldsymbol{\lambda}_V \tag{10}$$

$$\dot{\boldsymbol{\lambda}}_R = (\mu/r^3)\boldsymbol{\lambda}_V - (3\mu/r^5)\left(\boldsymbol{\lambda}_V^T \mathbf{r}\right)\mathbf{r} - \mathbf{A}_2 \boldsymbol{\lambda}_V - \mathbf{A}_3 \boldsymbol{\lambda}_V \tag{11}$$

$$\dot{\lambda}_m = T\boldsymbol{\lambda}_V^T \mathbf{1}_b/m^2 + \mathbf{A}_4 \boldsymbol{\lambda}_V \tag{12}$$

where $\mathbf{A}_1 = \partial \mathbf{a}_{\text{drag}}^T/\partial \mathbf{v}$, $\mathbf{A}_2 = \partial \mathbf{a}_{J_2}^T/\partial \mathbf{r}$, $\mathbf{A}_3 = \partial \mathbf{a}_{\text{drag}}^T/\partial \mathbf{r}$, and $\mathbf{A}_4 = \mathbf{a}_{\text{drag}}^T/m$. The first three matrices are listed in Appendix A for reference.

In burn arcs, the states $\mathbf{r}$, $\mathbf{v}$, and m and costates $\boldsymbol{\lambda}_R, \boldsymbol{\lambda}_V$, and λ_m are propagated using Eqs. (1) and (10–12). The switching function is $S = \boldsymbol{\lambda}_V^T \mathbf{1}_b/m - \lambda_m/c$. During coast arcs, the mass m and costate λ_m are constant. Therefore, the propagation of m and λ_m can be neglected, and the switching function is replaced by Eq. (13) [30]. Here θ_0 and θ denote the initial and current true anomalies of a coast arc. When $S'(\theta) \leq 0$, the trajectory will remain in a coast arc, whereas when $S'(\theta) > 0$, the trajectory will switch into a burn arc.

Note that if the atmospheric drag and J_2 accelerations cannot be neglected, this switching function will be replaced by the original one ($S = \boldsymbol{\lambda}_V^T \mathbf{1}_b/m - \lambda_m/c$). In this case, the proposed method will be used as an initial guess in the first homotopy [30]:

$$S'(\theta) = \|\boldsymbol{\lambda}_V(\theta)\| - \|\boldsymbol{\lambda}_V(\theta_0)\| \tag{13}$$

Switching Function Analysis

The duration of a coast arc can be much longer than that of a burn arc. The key for avoiding direct coast arc propagation is to make sure that the zero (θ_{zero}) found through a zero-finding algorithm is the first one. In this section, the result from the oscillation frequency analysis is combined with a zero-finding algorithm to solve the nonlinear equation $S'(\theta_{\text{zero}}) = 0$ and quickly locate the starting time of the next burn arc. If the eccentricity of a coast arc is zero (a circular orbit), there are infinite switching points [38]. This case will not be considered.

Oscillation Frequency of the Switching Function

Let us define the oscillation frequency of $\sin\theta$ or $\cos\theta$ to be a maximum of one with respect to the true anomaly. All the terms in the costate are related to sinusoid-type functions and thus will be analyzed with respect to sinusoids. For example, the frequencies of the functions $1 + \sin\theta$ and $10\cos\theta$ are at a maximum one, whereas those of $\sin^2\theta$, $\sin\theta/\cos\theta$, $\sin\theta\cos\theta$, and $\cos 2\theta - 5\sin\theta$ are at a maximum two.

Lemma 1: For a coast arc governed by the Keplerian model, the maximum oscillation frequencies of the position and velocity are two and one, respectively.

Proof: Based on Glandorf [31], the closed-form solution of a Keplerian motion is

$$\begin{bmatrix} \mathbf{r} \\ \mathbf{v} \end{bmatrix} = \begin{bmatrix} F_1\mathbf{I}_{3\times3} & F_2\mathbf{I}_{3\times3} \\ F_3\mathbf{I}_{3\times3} & F_4\mathbf{I}_{3\times3} \end{bmatrix} \frac{1}{H} \begin{bmatrix} F_4\mathbf{I}_{3\times3} & -F_2\mathbf{I}_{3\times3} \\ -F_3\mathbf{I}_{3\times3} & F_1\mathbf{I}_{3\times3} \end{bmatrix}_{t_0} \begin{bmatrix} \mathbf{r}_0 \\ \mathbf{v}_0 \end{bmatrix} \tag{14}$$

where t_0, $\mathbf{r}_0$, and $\mathbf{v}_0$ are the initial time, position, and velocity of a coast arc, respectively. In a Keplerian motion, the angular momentum magnitude H, semimajor axis a, eccentricity e, and semilatus rectum p are all constants. So, let us denote the constant part in the coast arc dynamics [Eq. (14)] as

$$\begin{bmatrix} \mathbf{r}_0' \\ \mathbf{v}_0' \end{bmatrix} = \frac{1}{H} \begin{bmatrix} F_4\mathbf{I}_{3\times3} & -F_2\mathbf{I}_{3\times3} \\ -F_3\mathbf{I}_{3\times3} & F_1\mathbf{I}_{3\times3} \end{bmatrix}_{t_0} \begin{bmatrix} \mathbf{r}_0 \\ \mathbf{v}_0 \end{bmatrix} \tag{15}$$

then the position $\mathbf{r}$ and velocity $\mathbf{v}$ are linear combinations of F_1 and F_2, F_3, and F_4, respectively [Eq. (16)]. Here, $F_1 = r\cos\theta$, $F_2 = r\sin\theta$, $F_3 = -(H/p)\sin\theta$, and $F_4 = (H/p)(e + \cos\theta)$.

$$\mathbf{r} = \mathbf{r}_0' F_1 + \mathbf{v}_0' F_2 \qquad \mathbf{v} = \mathbf{r}_0' F_3 + \mathbf{v}_0' F_4 \tag{16}$$

The position magnitude is $r = a(1 - e^2)/(1 + e\cos\theta)$. $F_1 = a(1 - e^2)/[(1/\cos\theta) + e]$ and $F_2 = a(1 - e^2)\sin\theta/(1 + e\cos\theta)$ have maximum oscillation frequencies of one and two, respectively, whereas F_3 and F_4 have a maximum frequency of one. Thus, the maximum oscillation frequencies of the position $\mathbf{r}$ and the velocity $\mathbf{v}$ are two and one, respectively.

Note that the maximum frequency calculated here is conservative. For example, it is obvious that the frequency of the position vector $\mathbf{r}$ is one and does not achieve the maximum two. In the switching function of a coast arc, a conservative maximum frequency requires more points to be sampled before the local region of the first zero point can be found. This property actually has advantages: 1) it will not miss the extreme case where the summation (multiplication) of a frequency n_1 mode and a frequency n_2 mode generates a $\max(n_1, n_2)$ ($n_1 + n_2$) frequency mode, and 2) the region where the first zero point is located is narrower and because of this the computational cost associated with the zero finding is reduced.

Lemma 2: For a coast arc governed by the Keplerian model, the maximum oscillation frequency of the switching function $S'(\theta)$ is eight.

Proof: The closed-form solution of costates in a coast arc is shown in Eq. (17), and it can be simplified as Eq. (18), where $[\boldsymbol{\lambda}_{V0}'^T \quad -\boldsymbol{\lambda}_{R0}'^T]^T = \mathbf{P}^{-1}(t_0)[\boldsymbol{\lambda}_{V0}^T \quad -\boldsymbol{\lambda}_{R0}^T]^T$. The matrices $\mathbf{P}(t)$ and $\mathbf{P}^{-1}(t_0)$ can be found in Glandorf [31]. Because the switching function $S'(\theta)$ only involves $\boldsymbol{\lambda}_V$, $\boldsymbol{\lambda}_R$ is neglected in the analysis. The switching function can be expanded as shown in Eq. (19) where $\mathbf{a}_i$, $i \in [1, 13]$ are determined by the position and velocity at the burn arc stop time or the coast arc starting time. The derivation can be found in Appendix B. Therefore, these vectors are all constants throughout the coast arc and the oscillation frequency is determined by 13 modes as shown in Eq. (19), where g and f are defined in Table 1 and F_6 can be

Table 1 Maximum frequency ($e \neq 1$)

Items	Max. frequency	Items	Max. frequency
F_1	1	F_3	1
F_2	2	F_4	1
$\mathbf{r}$	2	$r = a(1-e^2)/(1+e\cos\theta)$	1
$\mathbf{v}$	1	$g = [(p/h)(p+r)r\sin\theta - 3ept]/(1-e^2)$	3
F_6	0	$f = -(p/H)(p+r)r\cos\theta$	3
$F_1\mathbf{r}$	3	$\mathbf{H} = \mathbf{r}\times\mathbf{v}$ (const)	0
$F_6\mathbf{v}$	1	$g\mathbf{v}$	4
$F_2\mathbf{H}$	2	$F_1\mathbf{H}$	1
$F_2\mathbf{r}$	4	$f\mathbf{v}$	4
F_2^2	4	F_3F_6	1
F_1^2	2	gF_3	4
F_1F_2	3	fF_3	4
F_4F_6	1	fF_4	4
gF_4	4	$\boldsymbol{\lambda}_V$	4

found in Glandorf [31].

$$\begin{bmatrix} \boldsymbol{\lambda}_V \\ -\boldsymbol{\lambda}_R \end{bmatrix} = \mathbf{P}(t)\mathbf{P}^{-1}(t_0)\begin{bmatrix} \boldsymbol{\lambda}_{V0} \\ -\boldsymbol{\lambda}_{R0} \end{bmatrix} \tag{17}$$

$$\begin{bmatrix} \boldsymbol{\lambda}_V \\ -\boldsymbol{\lambda}_R \end{bmatrix} = \mathbf{P}(t)\begin{bmatrix} \boldsymbol{\lambda}'_{V0} \\ -\boldsymbol{\lambda}'_{R0} \end{bmatrix} \tag{18}$$

$$\begin{aligned}\boldsymbol{\lambda}_V &= [F_1\mathbf{r} - g\mathbf{v} \quad F_2\mathbf{r} - f\mathbf{v} \quad 2\mathbf{r} - F_6\mathbf{v}]\boldsymbol{\lambda}'_{V0} - [\mathbf{v} \quad F_1\mathbf{H} \quad F_2\mathbf{H}]\boldsymbol{\lambda}'_{R0} \\ &\triangleq \mathbf{a}_1F_1 + \mathbf{a}_2F_2 + \mathbf{a}_3F_3 + \mathbf{a}_4F_4 + \mathbf{a}_5F_1^2 + \mathbf{a}_6F_2^2 + \mathbf{a}_7F_1F_2 \\ &\quad + \mathbf{a}_8F_3F_6 + \mathbf{a}_9F_4F_6 + \mathbf{a}_{10}gF_4 + \mathbf{a}_{11}gF_4 + \mathbf{a}_{12}fF_3 + \mathbf{a}_{13}fF_4\end{aligned} \tag{19}$$

The maximum oscillation frequencies according to Lemma 1 are shown in Table 1. $\boldsymbol{\lambda}_V$ is a linear combination of these 13 modes, thus the maximum oscillation frequency of $\boldsymbol{\lambda}_V$ is four and the maximum frequency of the switching function $S'(\theta) = \|\boldsymbol{\lambda}_V(\theta)\| - \|\boldsymbol{\lambda}_V(\theta_0)\|$ is eight.

For a sinusoid-type wave, there are maximally three locations which intersect with the zero line (Fig. 2). Lemma 2 shows that the maximum frequency of the switching function is eight with respect to a sinusoid-type wave. Therefore, there are a maximum of 17 zeros for the switching function in an eccentric orbit (taking into account the start and endpoint of an orbit).

From now on, the proposed method is called the sampled method and the conventional propagation is the propagation method. There are three advantages if Lemma 2 is applied in finding the optimal multiple-burn trajectory.

The first advantage: Let us do a rough calculation to show the speed improvement by using this algorithm. For a coast arc with a semimajor axis of 7378 km (the period of this orbit is approximately 6307 s) and a fixed step size of 1 s used by the guidance code, 3154 points (in an average sense, 6307/2) will be evaluated before a switching point can be found. Using the sampled method, 17 points will be sampled at uniformly distributed true anomalies. After that, a region with 394 points (6307/16) will be used to locate a precise switching point. If 197 (394/2, in an average sense) points are evaluated (using a zero-finding algorithm), the computational time for a coast arc can be reduced up to $1 - (17 + 197)/3154 \approx 93.21\%$ compared with the direct propagating method. The reduction in the computation cost will be less because of the extra codes required, but the improvement is still significant.

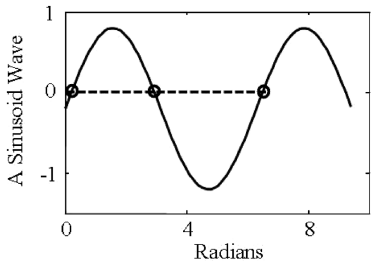

Fig. 2 A maximum of three zeros in a sinusoid function within one period.

The second advantage: In the propagation method, the precision of the switching point depends on the sampling rate, whereas in the sampled method, the precision depends on the tolerance of zero-finding algorithms, which can be the same as the machine precision.

The third advantage: The switching time (or true anomaly) of a coast arc can be regarded as optimization parameters where propagations of the coast arc can be avoided by using analytical solutions. However, the number of parameters to be optimized is increased. For example, if there are n coast arcs, the Jacobian matrices' dimension is $n + 7$ by $n + 7$ (n coast arc stop time plus position, velocity, and mass costates). Using the sampled algorithm, the gradient matrix size is still 7×7 which theoretically will reduce the number of iterations and the optimal solution will be less sensitive to the initial costate guess.

Switching Algorithm

To avoid significant atmospheric drag, the coast arc will be forced to switch to the next burn arc at a tolerant altitude h_{Tol}. θ_{dA} is denoted as the corresponding true anomaly at this tolerant altitude.

In Table 2, the algorithm is listed for calculating the 18 true anomalies (17 uniformly distributed true anomalies based on Lemma 2 and θ_{dA}) at locations where the switching function will be evaluated. The basic idea is to form a series of true anomalies considering θ_{dA} and the zero eccentricity case.

Table 3 lists the algorithm for finding the switching time true anomaly θ_{zero} (from a coast arc to a burn arc). Figure 3 shows the schematics of the switching algorithm. The switching function within the ith and $(i + 1)$th true anomalies is monotonic and includes a maximum of one zero. These sampled points are evaluated one by one until a positive switching function value is found. The zero-finding algorithm is modified based on the "fzero" function (in MATLAB®).

Summary of the Method

The summary of the method is demonstrated in Fig. 4. The solid line denotes the burn stage, whereas the dash line represents the coast stage. The first stage of the multiple burn-coast arcs can be either a burn or a coast arc [23]. There are two cases in which an initial coast arc should be avoided. First, in the case of a circular-to-circular coplanar mission, the length of an initial coast would be completely arbitrary in the sense that all initial coast durations are equally compatible with fuel optimality [23]. Secondly, there are cases in which mission geometry constraints preclude an optimal initial coast because it would result in a fall into the lower atmosphere or even

Table 2 True anomalies to be sampled in a coast arc

	Algorithm to find sampled true anomalies in a coast arc
1	If the coast arc orbital eccentricity is zero
2	Switch back to a burn arc immediately
3	Else
4	Find θ_{dA} (the true anomaly corresponding to the tolerant altitude)
5	End
6	If $\theta_0 < \pi$ or $\theta_{dA} < \theta_0$ (the Earth is on the right focus of the coast arc orbit)
7	$\theta_{dA} = 2\pi - \theta_{dA}$
8	End
9	A series of uniformly distributed true anomaly points θ_{sampled} within $[\theta_0, \theta_0 + 2\pi)$
10	Put θ_{dA} into θ_{sampled} where $\theta_{\text{sampled}} < \theta_{dA} < \theta_{\text{sampled},i+1}$, $i = 1, \ldots, 16$

Table 3 Switching algorithm

	Switching from a coast arc to a burn arc
1	Determining orbital elements at the coast arc starting point
2	Finding $N = 18$ sampled true anomaly locations using the algorithm in Table 2
3	Searching for a region $[i-1, i]$ where the switching function at location i is positive
4	If the switch values at all sampled locations are negative
5	The switching location true anomaly θ_{zero} is assumed to be θ_N
6	End
7	temp1 $= \theta_{i-1}$; temp2 $= \theta_i$
8	Forming a region [temp1, temp2] with the smaller value as temp1
9	Using a zero-finding algorithm to find the exact zero location
10	Making sure that the switching point is on the positive side of the zero
11	Finding the states and costates at the switching point

beneath the Earth surface [23]. The simulation cases in this paper belong to the above two cases and thus the first arc is set to be a burn arc. The last arc of the simulation may be a burn arc or a coast arc depending on the application. For example, in the Hohmann transfer-type trajectory, the last arc is a burn arc, whereas the last arc of a maximum ground track trajectory is a coast arc.

Numerical issues related to the implementation of the sampled method are discussed.

1) Dimensional models are used in both burn and coast arcs. Because the dynamic model in coast arcs is dimensional, the propagation from a burn arc to a coast arc is consistent.

2) It is convenient to regard the true anomaly, instead of time, as the independent variable in coast arcs. In the coast arc starting time, orbital elements (true anomaly, semimajor axis, eccentricity, semilatus rectum, and angular momentum) are obtained in relation to the position and velocity vectors. The detailed information for this transformation can be found in Prussing [40] or Xu [42].

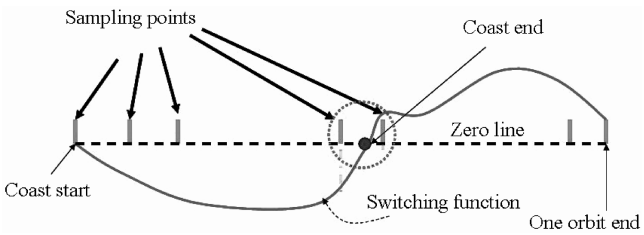

Fig. 3 Sampling algorithm schematics.

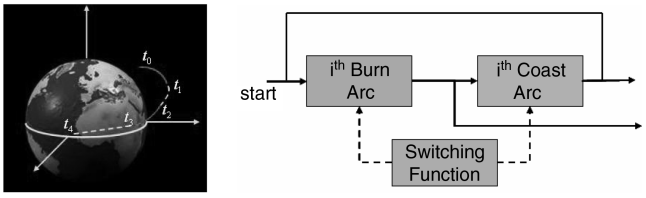

Fig. 4 Multi-burn-coast trajectory arc sequence.

3) To avoid numerical precision problems, the switching function needs to be tested in both arcs to make sure that the signs of the switching values are the same. For example, the switching value calculated in a burn arc is -1×10^{-12}, but it may be calculated as 1×10^{-15} in the next coast arc.

4) Furthermore, a tolerant altitude is added into the burn arc to avoid switches if the altitude of the vehicle is below this altitude. The purpose is to avoid a coast arc (if not the last arc) experiencing significant drag accelerations and increase the fidelity of using the analytical solution [14].

5) The atmospheric drag and J_2 is gradually introduced as an additional forcing term to the solution iteration.

Numerical Simulation

To demonstrate the effectiveness of the proposed algorithm, four examples are shown below. Software was written using MATLAB® and run in a Pentium IV computer (3 GHz CPU and 1 GB RAM). According to Gath [20], when code is written in C/C++ as opposed to MATLAB, the computational cost can be reduced to approximately 10%, or even less if codes are optimized. Therefore, the algorithm proposed in this paper can be used in real time. In these simulations, the computational time for coast arcs will be compared between two methods: one is the conventional propagation method, and the other is the sampled method. Also, the trajectory design performance will be evaluated using the error percentages of $|r_f - r_{\text{des},f}|/r_{\text{des},f}$ and $|v_f - v_{\text{des},f}|/v_{\text{des},f}$.

Hohmann Transfer Cases One and Two (Including the J_2 perturbation)

The first two examples are modified according to Vallado [43]. The initial orbit is circular with an altitude of 191,344.11 m. The final orbit is also circular with an altitude of 35,781,348.57 m. As seen in the initial and final orbits, the atmospheric drag can be safely ignored but the J_2 effect is considered in the simulation. The initial thrust-to-weight ratios used in these two simulations are 4.38 and 0.42, respectively. The initial costate guess can be obtained according to Redding [26]. The simulation results show that under the same achieved final orbit precision, the time spent using the sampled

Table 4 Simulation cases and results

Cases	T/W_0	Initial altitude, m	Final altitude, m	One iteration time, s			Achieved precision	
				Propagation	Sampling method	Time ratio	Position error %	Velocity error %
Hohmann transfer one	4.38	191,344.11	35,781,348.57	18.53	0.4688	2.5%	4.36	0.01
Hohmann transfer two	0.42	191,344.11	35,781,348.57	27.54	1.0625	3.8%	7.26	0.00
Low Earth orbit insertion	4.38	100 (yo-yo orbit)	100 (circular)		One burn arc only		0.00	0.34

method is only 2.5 and 3.8% of how much time the propagation method used.

As shown in Table 4, the case with low thrust performance is worse than the high thrust performance case, which is reasonable. Note that the time saved in the coast arc propagation has no relation to the final position and velocity error percentages.

Low Earth Orbit Insertion (Including the Atmospheric Drag and J_2 Perturbation)

This case shows a possible upper stage circular orbital insertion. The upper stage separation occurs at an altitude of 100 km from a vertical takeoff and vertical landing vehicle with an initial velocity of 0.471 km/s in the horizontal direction due to the Earth spin. The eccentricity of the initial orbit is almost one (nearly a yo-yo orbit) due to a nearly zero initial velocity. The final orbit needs to be a circular orbit with an altitude of 100 km. A more detailed problem description can be found in Xu [8]. The performance index is constructed to maximize the final mass $J = \varphi = m(t_f)$. For this circular orbital insertion, the terminal constraints $\boldsymbol{\Psi}$ are $\|\mathbf{v}_f\| - \|\mathbf{v}_{\text{des},f}\| = 0$, $\|\mathbf{r}_f\| - \|\mathbf{r}_{\text{des},f}\| = 0$, and $\mathbf{r}_f^T\mathbf{v}_f = 0$. The transversality conditions can be found through $\boldsymbol{\lambda}(t_f) = [\partial\varphi/\partial\mathbf{x} + (\partial\boldsymbol{\Psi}^T/\partial\mathbf{x})\boldsymbol{\upsilon}]_{t_f}$, where $\mathbf{x} = [\mathbf{r}^T, \mathbf{v}^T, m]^T$ and $\boldsymbol{\upsilon} \in \mathbb{R}^{3\times 1}$ is an unknown constant vector. The simulation shows that the proposed algorithm is flexible in dealing with the case where there is only one burn arc. The simulation results (the achieved precision) are compatible with those achieved from the "EFAT" methods [8].

As an example, Figs. 5–9 show the optimized trajectory results for the first Hohmann transfer case. The simulation results are similar for the second Hohmann transfer case and are not shown here. The switching function in a burn arc is always above zero. The altitude, mass flow, and velocity information are found in Figs. 6–8. The effects of the nonimpulsive thrusts can be seen in Fig. 9 because the second burn arc does not start at exactly a 180 deg true anomaly location as it would for the ideal cases. The value calculated in the simulation is 187.521 deg. The distance shown in Fig. 9 is dimensionless. For example, one means 1 times the radius of the Earth (approximately 6378 km). For the TGV orbital insertion simulation, there is no switching as shown in Fig. 10 and the remaining mass, velocity, and altitude histories as shown in Figs. 11–13.

Simple Analysis for the McCue Problem

McCue [39] used the quasilinearization method to solve the multiple-burn orbital transfer problem. The example used was described as a problem where the initial orbit is characterized by

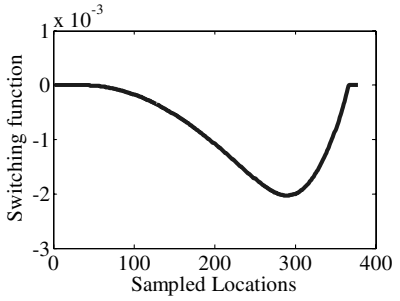

Fig. 5 Switching function for the Hohmann transfer case one.

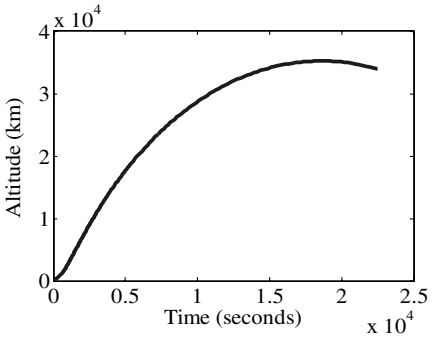

Fig. 6 Trajectory altitude for the Hohmann transfer case one.

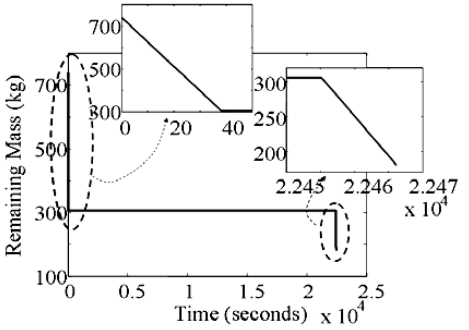

Fig. 7 Mass flow for the Hohmann transfer case one.

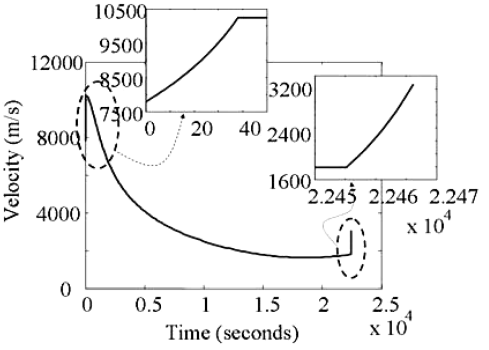

Fig. 8 Velocity for the Hohmann transfer case one.

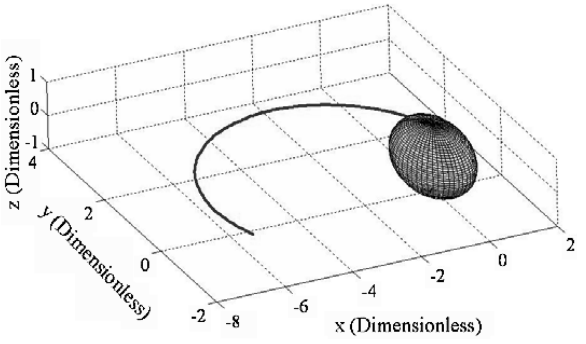

Fig. 9 Trajectory for Hohmann transfer case one.

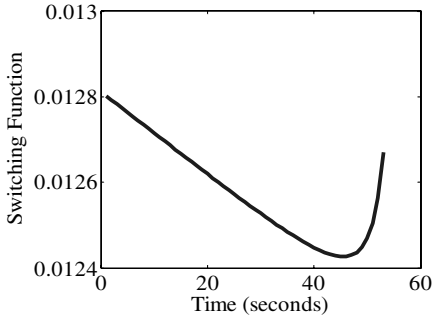

Fig. 10 Switching function for the TGV orbital insertion case.

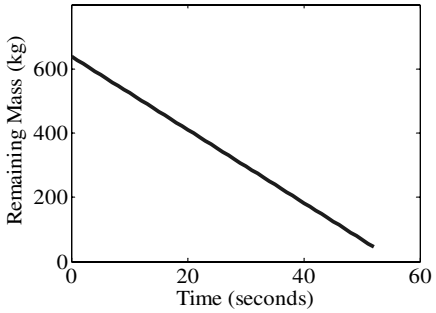

Fig. 11 Remaining mass for the TGV orbital insertion case.

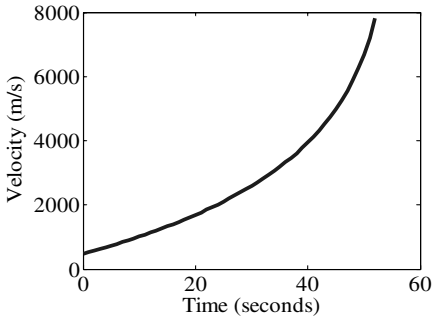

Fig. 12 Velocity for the TGV orbital insertion case.

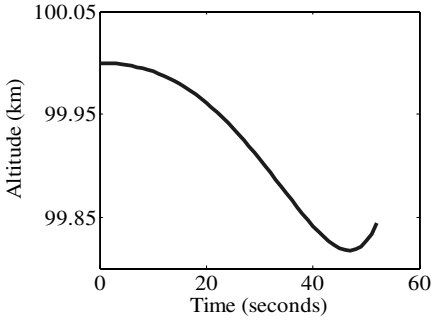

Fig. 13 Altitude for the TGV orbital insertion case.

$p = 8046.72$ km, $e = 0.2$, and $\omega = -90$ deg and the target orbit is characterized by $p = 9656.06$ km, $e = 0.2$, and $\omega = 30$ deg. To achieve adequate convergence using quasilinearization, the switching time must be located at a precision of 0.001 s [39] at least. In McCue, the switching time is still used as one of the optimization parameters and the approximate switching time found from impulse solutions is regarded as the initial guess. During optimization iteration, a zero-finding algorithm was used to search for a switching point around this guess. If the newfound switching time deviates too much from the previous one, the new one will not be used. The propagation time in the coast arc is nearly 5400 s with a sampling rate at 1000 Hz [39]. If the switching analysis method proposed in this paper is used, the sampled points will be reduced and a better precision can be achieved by the zero-finding algorithm.

Conclusions

Designing a rapid optimal multiple-burn trajectory is a challenging task. The optimal result is sensitive to the initial costate guess and the computational cost is high. The computational cost stems from 1) a relatively high cost in trajectory propagations (simulation of a trajectory) and 2) the number of trajectories (computation of gradient information) that have to be iterated in order to find the optimal solution. The method proposed is different from most other works. Through the oscillation frequency study of the switching function, the propagation of the coast arc is avoided and replaced by a zero-finding program without zeros' leakage. The numerical implementation of this algorithm is discussed and four trajectory designs were simulated to show the effectiveness of the proposed algorithm: two Hohmann transfer-type orbital transfers, a low Earth orbital insertion, and the McCue's two burn elliptic orbital transfer problem. The simulation results show an average of 96.8% computational time reduction in the coast arc.

Appendix A: Derivatives

1) $\mathbf{A}_1 = \partial \mathbf{a}_{\text{drag}}^T / \partial \mathbf{v}$ when $\|\mathbf{v}\| \geq 340$ m/s:

$$\frac{\partial \mathbf{a}_{\text{drag},j}}{\partial v_i} = c_2 \begin{cases} \|\mathbf{v}\| + v_i^2/\|\mathbf{v}\| & \text{if } i = j \\ v_i v_j / \|\mathbf{v}\| & \text{if } i \neq j \end{cases} \qquad i, j = 1, 2, 3 \quad \text{(A1)}$$

2) $\mathbf{A}_2 = \partial \mathbf{a}_{J_2}^T / \partial \mathbf{r}$:

$$\frac{\partial \mathbf{a}_{J_2,j}^T}{\partial r_i} = c_1/(2r^9) \begin{cases} (3r^4 - 15r^2z^2 - 15r^2r_i^2 + 105r_i^2z^2) & \text{if } i = j = 1, 2 \\ (9r^4 - 90r^2z^2 + 105z^4) & \text{if } i = j = 3 \\ (-15xyr^2 + 105xyz^2) & \text{if } i = 1, j = 2 \\ (-45r_izr^2 + 105r_iz^3) & \text{if } i = 1, 2, j = 3 \end{cases} \quad \text{(A2)}$$

3) $\mathbf{A}_3 = \partial \mathbf{a}_{\text{drag}}^T / \partial \mathbf{r}$

$$\frac{\partial \rho}{\partial h} = -1.27429124836 \times 10^{26} (141.89 + 0.00299h)^{-13.388} \quad \text{(A3)}$$

$h \geq 25$ km

$$\frac{\partial \mathbf{a}_{\text{drag},j}^T}{\partial r_i} = -\frac{1}{2m} C_D A \|\mathbf{v}\| v_j \frac{\partial \rho}{\partial h} \frac{r_i}{\|\mathbf{r}\|} \qquad i, j = 1, 2, 3 \quad \text{(A4)}$$

Appendix B: Simplification of the Switching Function

The analytical solutions of state and costate are given by

$$\mathbf{r} = \mathbf{r}_0' F_1 + \mathbf{v}_0' F_2 \qquad \mathbf{v} = \mathbf{r}_0' F_3 + \mathbf{v}_0' F_4 \quad \text{(B1)}$$

and

$$\begin{bmatrix} \boldsymbol{\lambda}_V \\ -\boldsymbol{\lambda}_R \end{bmatrix} = \mathbf{P}(t) \begin{bmatrix} \boldsymbol{\lambda}_{V0}' \\ -\boldsymbol{\lambda}_{R0}' \end{bmatrix} \quad \text{(B2)}$$

In analyzing the switching function, the concerned part of the costate dynamics is given by Eq. (B3), where g and f are defined in Table 1.

$$\boldsymbol{\lambda}_V = [F_1\mathbf{r} - g\mathbf{v} \quad F_2\mathbf{r} - f\mathbf{v} \quad 2\mathbf{r} - F_6\mathbf{v}]\boldsymbol{\lambda}_{V0}' - [\mathbf{v} \quad F_1\mathbf{H} \quad F_2\mathbf{H}]\boldsymbol{\lambda}_{R0}' \quad \text{(B3)}$$

Substituting Eq. (B2) into Eq. (B3), Eq. (B4)is achieved, where $\boldsymbol{\lambda}'_{V0} = [\lambda'_{V0,1}, \lambda'_{V0,2}, \lambda'_{V0,3}]^T$ and $\boldsymbol{\lambda}'_{R0} = [\lambda'_{R0,1}, \lambda'_{R0,2}, \lambda'_{R0,3}]^T$.

$$\begin{aligned}
\boldsymbol{\lambda}_V &= [F_1\mathbf{r} - g\mathbf{v}\ F_2\mathbf{r} - f\mathbf{v}\ 2\mathbf{r} - F_6\mathbf{v}]\boldsymbol{\lambda}'_{V0} - [\mathbf{v}\ F_1\mathbf{H}\ F_2\mathbf{H}]\boldsymbol{\lambda}'_{R0} \\
&= \left[\mathbf{r}'_0\left(F_1^2 - gF_3\right) + \mathbf{v}'_0(F_1F_2 - gF_4)\right]\lambda'_{V0,1} - \left[\mathbf{r}'_0F_3\right. \\
&\quad \left. + \mathbf{v}'_0F_4\right]\lambda'_{R0,1} + \left[\mathbf{r}'_0(F_1F_2 - fF_3) + \mathbf{v}'_0\left(F_2^2 - fF_4\right)\right]\lambda'_{V0,2} \\
&\quad - [F_1\mathbf{H}]\lambda'_{R0,2} + [\mathbf{r}'_0(2F_1 - F_3F_6) + \mathbf{v}'_0(2F_2 - F_4F_6)]\lambda'_{V0,3} \\
&\quad - [F_2\mathbf{H}]\lambda'_{R0,3} = (2\lambda'_{V0,3}\mathbf{r}'_0 - \lambda'_{R0,2}\mathbf{H})F_1 + (2\lambda'_{V0,3}\mathbf{v}'_0 \\
&\quad - \lambda'_{R0,3}\mathbf{H})F_2 + (-\mathbf{r}'_0\lambda'_{R0,1})F_3 + (-\mathbf{v}'_0\lambda'_{R0,1})F_4 + (\lambda'_{V0,1}\mathbf{r}'_0)F_1^2 \\
&\quad + (\lambda'_{V0,2}\mathbf{v}'_0)F_2^2 + (\lambda'_{V0,1}\mathbf{v}'_0 + \lambda'_{V0,2}\mathbf{r}'_0)F_1F_2 + (-\lambda'_{V0,3}\mathbf{r}'_0)F_3F_6 \\
&\quad + (-\lambda'_{V0,3}\mathbf{v}'_0)F_4F_6 + (-\lambda'_{V0,1}\mathbf{r}'_0)gF_3 + (-\lambda'_{V0,1}\mathbf{v}'_0)gF_4 \\
&\quad + (-\lambda'_{V0,2}\mathbf{r}'_0)fF_3 + (-\lambda'_{V0,2}\mathbf{v}'_0)fF_4 \triangleq \mathbf{a}_1F_1 + \mathbf{a}_2F_2 + \mathbf{a}_3F_3 \\
&\quad + \mathbf{a}_4F_4 + \mathbf{a}_5F_1^2 + \mathbf{a}_6F_2^2 + \mathbf{a}_7F_1F_2 + \mathbf{a}_8F_3F_6 + \mathbf{a}_9F_4F_6 \\
&\quad + \mathbf{a}_{10}gF_3 + \mathbf{a}_{11}gF_4 + \mathbf{a}_{12}fF_3 + \mathbf{a}_{13}fF_4 \qquad \text{(B4)}
\end{aligned}$$

Note that the defined vectors $\mathbf{a}_i$, $i = 1, \ldots, 13$ are all constant vectors determined by the burn stop time position and velocity vectors. Therefore, during the coming coast arc after this burn arc, these vectors will be constant and the oscillation frequencies will be fully determined by the modes.

Acknowledgements

This research was supported by TGV Rockets, Inc. The author gratefully acknowledges the reviewers and the Associate Editor for their suggestions.

References

[1] Lawden, D. F., "Fundamentals of Space Navigation," *Journal of the British Interplanetary Society*, Vol. 13, March 1954, pp. 87–101.

[2] Lawden, D. F., *Optimal Trajectories for Space Navigation*, Butterworths, London, 1963, pp. 54–68.

[3] Leitmann, G., *An Introduction to Optimal Control*, McGraw–Hill, New York, 1966, pp. 151–155.

[4] Marec, J. P., *Optimal Space Trajectories*, Elsevier, Amsterdam, The Netherlands, 1979, p. 329.

[5] Jezewski, D. J., "Primer Vector Theory and Applications," NASA TR R-454, NASA Johnson Space Flight Center, Houston, TX, 1975.

[6] Calise, A. J., Melamed, N., and Lee, S., "Design and Evaluation of a Three-Dimensional Optimal Ascent Guidance Algorithm," *Journal of Guidance, Control, and Dynamics*, Vol. 21, No. 6, 1998, pp. 867–875.

[7] Lu, P., "Use of Approximate Gradients in Trajectory Optimization," *Journal of Guidance, Control, and Dynamics*, Vol. 15, No. 5, 1992, pp. 1299–1301.

[8] Xu, Y., "Trajectory Control and Analysis for the Vertical Takeoff and Vertical Landing Reusable Launch Vehicle's Upper Stage," AIAA Paper 2005-5996, 2005.

[9] Pontryagin, L. S., Boltyanskii, V., Gamkrelidze, R., and Mishchenko, E., *The Mathematical Theory of Optimal Processes*, Pergamon, New York, 1964, pp. 239–256.

[10] Bell, D. J., "Optimal Space Trajectories—A Review of Published Work," *Aeronautical Journal of the Royal Aeronautical Society*, Vol. 72, Feb. 1968, pp. 141–146.

[11] Lawden, D. F., "Rocket Trajectory Optimization: 1950–1963," *Journal of Guidance, Control, and Dynamics*, Vol. 14, No. 4, July–Aug. 1991, pp. 705–711.

[12] Betts, J. T., "Survey of Numerical Methods for Trajectory Optimization," *Journal of Guidance, Control, and Dynamics*, Vol. 21, No. 2, March–April 1998, pp. 193–207.

[13] Ocampo, C., "Finite Burn Maneuver Modeling for a Generalized Spacecraft Trajectory Design and Optimization System," *Annuals of the New York Academy of Sciences*, Vol. 1017, May 2004, pp. 210–233.

[14] Brown, K. R., and Johnson, G. W., "Rapid Computation of Optimal Trajectories," *IBM Journal of Research and Development*, Vol. 11, No. 4, 1967, pp. 373–382.

[15] Betts, J. T., and Cramer, E. J., "Application of Direct Transcription to Commercial Aircraft Trajectory Optimization," *Journal of Guidance, Control, and Dynamics*, Vol. 18, No. 1, Jan.–Feb. 1995, pp. 151–159.

[16] Enright, P. J., and Conway, B. A., "Optimal Finite-Thrust Spacecraft Trajectories Using Collocation and Nonlinear Programming," *Journal of Guidance, Control, and Dynamics*, Vol. 14, No. 5, 1991, pp. 981–985.

[17] Hargraves, C. R., and Paris, S. W., "Direct Trajectory Optimization Using Nonlinear Programming and Collocation," *Journal of Guidance, Control, and Dynamics*, Vol. 10, No. 4, July–Aug. 1987, pp. 338–342.

[18] Zondervan, K. P., Wood, L. J., and Caughey, T. K., "Optimal Low-Thrust, Three-Burn Orbit Transfers with Large Plane Changes," *Journal of the Astronautical Sciences*, Vol. 32, No. 3, 1984, pp. 407–427.

[19] Ilgen, M. R., "A Hybrid Method for Computing Optimal Low-Thrust OTV Trajectories," AAS Paper 94-129, 1994.

[20] Gath, P. F., "Improvements to a Hybrid Algorithm for Rapid Generation of 3-D Optimal Launch Vehicle Ascent Trajectories," Diploma Thesis, IFR_SR_98_016, Institute of Flight Mechanics and Control, University of Stuttgart, Stuttgart, Germany, Dec. 1998.

[21] Betts, J. T., and Huffman, W. P., "Trajectory Optimization on a Parallel Processor," *Journal of Guidance, Control, and Dynamics*, Vol. 14, No. 2, March–April 1991, pp. 431–439.

[22] Brusch, R. G., "Constrained Impulsive Trajectory Optimization for Orbit-to-Orbit Transfer," *Journal of Guidance, Control, and Dynamics*, Vol. 2, No. 3, May–June 1979, pp. 204–212.

[23] Brown, K. R., Harrold, E. F., and Johnson, G. W., "Rapid Optimization of Multiple-Burn Rocket Flights," NASA Report CR-1430, Washington, D. C., Sept. 1969.

[24] Jezewski, D. J., "Optimal Analytic Multiburn Trajectories," *AIAA Journal*, Vol. 10, No. 5, May 1972, pp. 680–685.

[25] Kornhauser, A. L., Lion, P. M., and Hazelrigg, G. A., "An Analytic Solution for Constant-Thrust, Optimal-Coast, Minimum-Propellant Space Trajectories," *AIAA Journal*, Vol. 9, No. 7, July 1971, pp. 1234–1239.

[26] Redding, D. C., "Highly Efficient, Very Low-Thrust Transfer to Geosynchronous Orbit: Exact and Approximate Solutions," *Journal of Guidance, Control, and Dynamics*, Vol. 7, No. 2, March–April 1984, pp. 141–147.

[27] Gath, P. F., and Calise, A. J., "Optimization of Launch Vehicle Ascent Trajectories with Path Constraints and Coast Arcs," *Journal of Guidance, Control, and Dynamics*, Vol. 24, No. 2, March–April 2001, pp. 296–304.

[28] Kelley, H. J., Uzzell, B. R., and McKay, S. S., "Rocket Trajectory Optimization by a Second-Order Numerical Technique," *AIAA Journal*, Vol. 7, No. 5, 1969, pp. 879–884.

[29] Chuang, C. H., Goodson, T. D., Ledsinger, L. A., and Hanson, J., "Optimality and Guidance for Planar Multiple-Burn Orbit Transfers," *Journal of Guidance, Control, and Dynamics*, Vol. 19, No. 6, Nov.–Dec. 1996, pp. 1310–1316.

[30] Dukeman, G. A., and Calise, A. J., "Enhancements to an Atmospheric Ascent Guidance Algorithm," AIAA Paper 2003-5638, 2003.

[31] Glandorf, D. R., "Lagrange Multipliers and the State Transition Matrix for Coasting Arcs," *AIAA Journal*, Vol. 7, No. 2, 1969, pp. 363–365.

[32] Lewallen, J. M., Schwausch, O. A., and Tapley, B. D., "Coordinate System Influence on the Regularized Trajectory Optimization Problem," *Journal of Spacecraft and Rockets*, Vol. 8, No. 1, Jan. 1971, pp. 15–20.

[33] Kechichian, J. A., "Trajectory Optimization Using Eccentric Longitude Formulation," *Journal of Spacecraft and Rockets*, Vol. 35, No. 3, May–June 1998, pp. 317–326.

[34] Kechichian, J. A., "Mechanics of Trajectory Optimization Using Nonsingular Variational Equations in Polar Coordinates," *Journal of Guidance, Control, and Dynamics*, Vol. 20, No. 4, July–Aug. 1997, pp. 812–818.

[35] Fernandes, S. d. S., "Universal Closed-Form of Lagrangian Multipliers for Coast Arcs of Optimum Space Trajectories," *Journal of Brazilian Society of Mechanical Sciences and Engineering*, Vol. 25, No. 4, Oct.–Dec. 2003, pp. 1–14.

[36] Markley, F. L., "Approximate Cartesian State Transition Matrix," *The Journal of the Astronautical Sciences*, Vol. 34, No. 2, April–June 1996, pp. 161–169.

[37] Wirthman, D. J., Park, S. Y., and Vadali, S. R., "Trajectory Optimization Using Parallel Shooting Method on Parallel Computer," *Journal of Guidance, Control, and Dynamics*, Vol. 18, No. 2, 1995, pp. 377–379.

[38] Carter, T. E., "Effects of Propellant Mass Loss on Fuel-Optimal Rendezvous Near Keplerian Orbit," *Journal of Guidance, Control, and Dynamics*, Vol. 12, No. 1, Jan.–Feb. 1989, pp. 19–26.

[39] McCue, G. A., "Quasilinearization Determination of Optimum Finite-Thrust Orbital Transfer," *AIAA Journal*, Vol. 5, No. 5, April 1967, pp. 755–763.

[40] Prussing, J. E., and Conway, B. A., *Orbital Mechanics*, Oxford Univ. Press, Oxford, England, U.K., 1993, pp. 164–168.
[41] Anderson, J. D., *Aircraft Performance and Design*, McGraw–Hill, New York, 1999, p. 67.
[42] Xu, Y., "Dynamics and Control for Formation Flying System," Ph.D. Dissertation, University of Florida, Gainesville, FL, Dec. 2003, Chap. 2.
[43] Vallado, D. A., *Fundamentals of Astrodynamics and Applications*, 2nd ed., Space Technology Library, Kluwer Academic, Boston, MA, 2004, pp. 314–315.

C. McLaughlin
Associate Editor